Physico-chemical and mechanical properties of microencapsulated phase change material

Jessica Giro-Paloma[a] , Gerard Oncins [b], Camila Barreneche [a,c,] , Mònica Martínez [a], A. Inés Fernández [a], Luisa F. Cabeza [c]

[a] Universitat de Barcelona, Faculty of Chemistry, Department of Materials Science and Metallurgical Engineering, C/Martí i Franquès, 1, 08028 Barcelona, Spain
[b] Centres Científics i Tecnològics de la Universitat de Barcelona (CCiTUB), C/Lluís Solé i Sabarís, 1, 08028 Barcelona, Spain
[c] GREA Innovació Concurrent, Edifici CREA, Universitat de Lleida, C/Pere de Cabrera s/n, 25001 Lleida, Spain

Abstract

Microencapsulated phase change materials (MPCM) are well known in advanced technologies for the utilization in active and passive systems, which have the capacity to absorb and slowly release the latent heat involved in a phase change process. Microcapsules consist of little containers, which are made of polymer on the outside, and paraffin wax as PCM in the inside. The use of microencapsulated PCM has many advantages as microcapsules can handle phase change materials as core allowing the preparation of slurries. However there are some concerns about cycling of MPCM slurries because of the breakage of microcapsules during charging/discharging and the subsequent loss of effectiveness. This phenomenon motivates the study of the mechanical response when a force is applied to the microcapsule. The maximum force that Micronal® DS 5001 can afford before breaking was determined by Atomic Force Microscopy (AFM). To simulate real conditions in service, assays were done at different temperatures: with the PCM in solid state at 25 ºC, and with the PCM melted at 45 ºC and 80 ºC. To better understand the behavior of these materials, Micronal® DS 5001 microcapsules were characterized using different physic-chemical techniques. Microcapsules Fourier Transform Infrared Spectroscopy (FT-IR) results showed the main vibrations corresponding to acrylic groups of the outside polymer. Thermal stability was studied by Thermogravimetrical Analysis (TGA), and X-ray Fluorescence (XRF) was used to characterize the resulting inorganic residue. The thermal properties were determined using Differential Scanning Calorimetry (DSC) curves. Particles morphology was studied with Scanning Electron Microscopy (SEM) and Mie method was used to evaluate the particle size distribution. Samples had a bimodal distribution of size and were formed by two different particles sizes: agglomerates of 150 μm diameter formed by small particles of 6 μm. Atomic Force Microscopy in nanoindentation mode was used to evaluate the elastic response of the particles at different temperatures. Different values of effective modulus E_{eff} were calculated for agglomerates and small particles. It was observed that stiffness depended on the temperature assay and particle size, as agglomerates showed higher stiffness than small particles, which showed an important decrease in elastic properties at 80 ºC.

1. Introduction

The phase change materials (PCMs) for thermal energy storage (TES) [1] must have both high latent heat and thermal conductivity as the main properties [2,3]. It has been found that with the help of PCMs the indoor temperature fluctuations can be reduced significantly whilst maintaining desirable thermal comfort [4,5]. Materials studied for this application are hydrated salt [6], paraffin waxes [7–9], fatty acids [10–13], fatty alcohols [14] and eutectics of organic and non-organic compounds [15,16]. Microencapsulated phase change materials [17] (MPCM) are used in composite formulations for thermal energy storage in passive systems or in active systems as aqueous slurries.

Microencapsulation is a process whereby small, spherical or rod-shaped particles are enclosed in a thin, high molecular weight polymeric film. Microcapsules are little containers made by a hydrophobic core material (phase change material, PCM) and a polymeric hard shell [18]. The advantages of MPCM are the protection against influences of the outside environment, the increase of the specific heat-transfer area, and improved tolerance to volume changes. Microencapsulation has been widely used to make copying paper, functional textiles, preservation or targeted delivery of chemical, food, etc.

In this study Micronal® DS 5001 from BASF® with a melting temperature between 26 and 27 ºC was used. The application temperature range of the selected product was tailored particularly to its employment in buildings (10–30 ºC). Micronal® has been incorporated in mortars, concrete or plasterboard as passive systems [19–21], and it is also used in active systems as slurries [22–29]. A better understanding of its performance and limitations in these systems needs more knowledge of the material properties, mainly thermal as well as chemical or mechanical roperties. In its usage as slurries, the mechanical behavior of the microcapsules becomes a key issue during charging/discharging, as the mechanical integrity of the shell is essential for its performance during thermal cycling and pumping. When Micronal® is used as aqueous slurry in active storage systems, changes are observed after several thermal cycles that are attributed to a partial degradation of the microcapsules by breakage [30]. Therefore, this study has two main objectives: the first one is the characterization of chemical and physical properties of Micronal® DS 5001 like surface area, particle size distribution, and chemical composition. The second objective is the characterization of the mechanical performance of microcapsules at different temperatures using Atomic Force Microscope (AFM). This characterization should help us to better understand the behavior of Micronal® in the above cited applications.

2. Materials and methods

The physico-chemical characterization of Micronal® DS 5001 consisted in the determination of density, Specific BET surface area, and particle size distribution. Infrared spectroscopy (FT-IR) and X-Ray Fluorescence spectroscopy (XRF) were performed with Thermogravimetrical Analysis (TGA) to complete the chemical characterization. Thermal properties were evaluated with differential scanning calorimeter, and scanning electron microscopy was used to study the morphology of the sample.

2.1. Physicochemical characterization

2.1.1. Density and BET specific surface

Density was measured with a Micrometrics® Pycnometer AccuPyc 1330 at 24 ºC and the specific surface BET was measured by Micrometrics® (TriStar 3000).

2.1.2. Particle size distribution

The sample was analyzed using a Beckman Coulter® LS™ 13 320 with Universal Liquid Module. The results were analyzed using the mathematical models Fraunhofer and Mie, as the use of one or the other depends on the particle size and the opacity of the material. The Fraunhofer model is used for opaque particles bigger than 30 μm, whereas the Mie model fits better for homogenous and spherical particles, opaque or transparent and with diameters be- low 30 μm [31].

2.1.3. Fourier transform infrared spectroscopy (FT-IR)

FT-IR spectroscopy is a powerful technique to identify func- tional groups in organic polymers or compounds. It was done through FT-IR Bomem ABB FTLA using a working range from 350 to 4000 cm^{-1}.

2.1.4. X-Ray Fluorescence (XRF)

X-ray fluorescence semi-quantitative analysis was performed on the calcined residue of Micronal® sample. A spectrophotometer Panalytical Philips PW 2400 sequential X-ray equipped with the software UniQuant® V5.0 was used.

2.1.5. Thermogravimetrical Analysis (TGA)

Thermal stability of the microcapsules was evaluated with a Simultaneous SDTQ600 TA Instruments under air atmosphere. The scanning rate was 0.5 K/min in the temperature range between 25 and 30 ºC followed by an isothermal step during 300 min. Then, temperature was increased at 1 K/min from 30 to 100 ºC, followed by an isothermal step during 300 min. The last heating ramp was at 5 K/min from 100 to 600 ºC.

2.2. Thermal properties with Differential Scanning Calorimetry (DSC)

The most common methods used in DSC analysis of PCM are dynamic method and step method. The dynamic method consists on heating or cooling the sample at a constant rate while the heat flux of the sample is measured [32,33]. Generally, when the dynamic method is applied, the phase transition is not an isothermal process because the thermal equilibrium is not achieved. A possible option to solve this problem is collecting the data using the step method, where the heating rate is changed by temperature intervals (steps).

The thermal properties such as melting/solidification temperature and melting/solidification enthalpy of the microcapsules containing PCM were evaluated by the Research Group Grea at the University of Lleida, using both methods by DSC with a *DSC 822- e* from Mettler Toledo. An aluminum crucible of 40 μl under N_2 atmosphere flow of 80 mL/min was used. The heating rate used was 0.5 ºC/min in both methodologies. This technique shows the melting temperature (T_m) and solidification temperature (T_s) of the sample and the enthalpy value for each process (melting and solidification, H_m and H_s respectively) which is equivalent to the area under the curve.

2.3. Scanning Electron Microscopy (SEM)

The morphology of the sample was characterized using an environmental scanning electron microscope (ESEM, Quanta 200 FEI, XTE 325/D8395). The sample was stuck on the sample holder using a double-sided tape and then the particle size and the morphology of the sample was observed. The working conditions were low vacuum and high voltage (15 kV), and the image obtained by secondary electrons.

2.4. Stiffness characterization by atomic force microscopy

To determine the mechanical properties of the sample of Micronal® DS 5001, AFM was performed at Scientific and Technological Centers of the Universitat de Barcelona (CCiTUB). AFM probes radius (R) was measured using the SPIP reconstruction software. R value was measured before and after every mechanical test in or- der to ensure that the tip shape did not change due to plastic deformation, which would invalidate stiffness value measurements through effective Young Modulus (E_{eff}).

AFM topographic images were acquired in intermittent contact mode using a MFP-3D system (Asylum Research). For this sort of measurements, Micronal® particles were glued on a metallic disk with epoxy. Care was taken to avoid an excess of glue around the particles that may result in a noticeable change in their mechanical properties. By means of the optical system attached to the AFM, only clean and spherical particles were chosen to be studied.

Topographic measurements as well as mechanical tests on Micronal® DS 5001 particles were performed with a diamond tip mounted on a stainless steel cantilever with a nominal k value of 265 nN/nm (Veeco). Nevertheless, k values of probes were individually measured by means of the thermal noise routine implemented in the software [34].

Mechanical measurements were performed with the Force Spectroscopy mode, using the AFM probe as a nanoindenter. As the goal of this experimental study is to assess the E_{eff} value, vertical forces applied by the AFM probe (F) were tuned so as to always remain in the elastic deformation region.

Two different sample sets were tested; one of them consisted on Micronal® particle aggregates exceeding 100 μm in diameter (agglomerates) and the other consisted on particles with diameters below 10 μm (small particles). The necessary F value to break the agglomerates and the small spheres was studied, so plastic deformation was topographically detected to take place at F values around 5 μN for the agglomerates and at 3 μN for the small particles; therefore measurements presented in this work were acquired at F values of 3 μN and 1.5 μN for the two different sets of

particles, respectively. The elastic–plastic transition tested by AFM is depicted in Fig. 1 in a small particle without applying load (no contact), and after applying load (deformation of the sample). Fig. 1 shows the vertical force *vs*. sample penetration curve obtained by processing the measurement of the cantilever deflection as it moves to the sample when a F value of 7 μN was applied (continuous line corresponds to tip sample approach process and dot- ted line corresponds to the tip retraction from the sample). It was the maximum F exerted, so plastic deformation was induced on the particle. The first region (flat, Fig. 1a) corresponds to the lack of contact between tip and sample. When contact is reached, the cantilever applies an increasing F on the sample, deforming it
elastically.

The deformation process is depicted from Fig. 1a–c. So, Fig. 1a shows no contact between tip and the small particles. Then at a certain sample penetration value, F suddenly decreases as it can be seen in Fig. 1b, confirming the plastic penetration of the sample. As F and sample penetration continue increasing (Fig. 1c), the sample is further deformed. The retraction of the AFM probe is depicted by the dotted line. In this specific experiment, the F value needed to plastically deform the sample is approximately 4 μN.

Individual indentation experiments were performed in different spots of the upper flat-top part of Micronal® particles in order to avoid tip slippage due to sample curvature. F is calculated as in Eq. (1), where k is the AFM probe, and D_z is cantilever deflection in the z axis:

$$F = k \ D_z \quad (1)$$

The cantilever deflection is expressed in Eq. (2), where DV is the increment in photodetector vertical signal as the tip contacts the sample and S is the sensitivity, which is the slope of the contact region of a force curve performed on a rigid sample:

$$D_z = DV/S \quad (2)$$

The sample penetration (d) due to the exerted F value is evaluated as Eq. (3), where z represents the piezo-scanner displacement in the axis perpendicular to the sample plane:

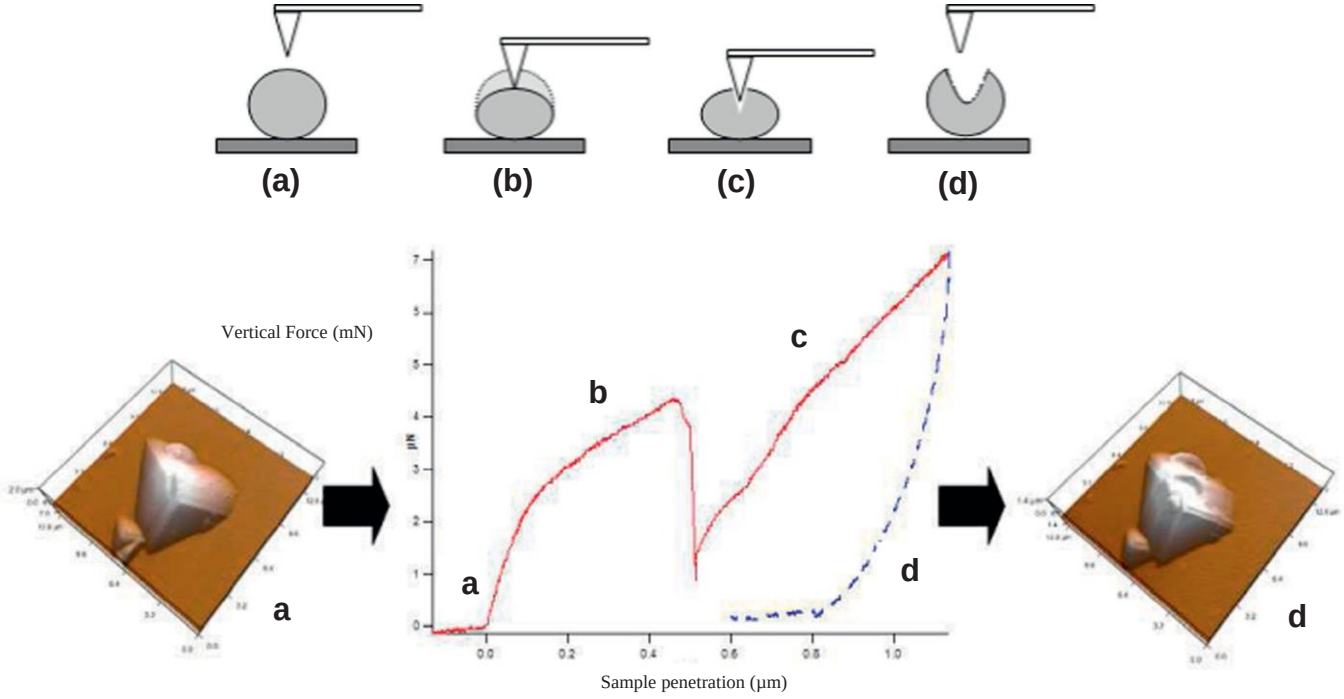

Fig. 1. Mechanical testing of the elastic-plastic region by AFM of a small particle, (a) no contact; (b) plastic penetration; (c) deformation of the sample; and (d) the retraction of the AFM probe.

$$d = z - D_z \quad (3)$$

F vs. *z* curves obtained at a certain *F* value were analyzed using the Hertz model in the elastic region by means of Eq. (4), and effective Modulus (E_{eff}) value can be obtained using Eq. (5):

$$F = (3/4)\, E_{eff}\, R^{1/2}\, d^{3/2} \quad (4)$$

$$1/E_{eff} = [(1 - \nu^2)/E] + [(1 - \nu_i^2)/E_i] \quad (5)$$

where ν is the Poisson ratio with a value of 0.33. Subindex *i* corresponds to the mechanical properties of the SiO_2 *AFM* probe (E_i = 76 GPa [35]) and ν_i = 0.17 [36].

It is important to notice that a triangular dent in the top of the particle can be seen when it is plastically deformed by the AFM probe. The general shape of the particles also appears to be triangular; this corresponds to the shape of the AFM tip, which is pyramidal, and not to the real shape of the particle. Individual indentation experiments were performed in different spots of the upper flat-top part of Micronal® particles in order to avoid tip slippage due to sample curvature.

3. Results and discussion

3.1. Physicochemical characterization

3.1.1. Density and specific BET surface

The result of average density is 0.995 ± 0.003 g/cm³. This value reflects the average density of two different materials: the density of the polymeric shell (1.0–1.2 g/cm³) and the density of the paraffin wax core (0.76–0.88 g/cm³).

The result of the BET surface area was 2.61 ± 0.04 m²/g; this value is adequate to be used as filler in the polymer matrix, as values below 5 m²/g are recommended to guarantee the effectiveness of a mixing process [37].

3.1.2. Particle size distribution

The calculations covered a range from 0.04 to 2000 μm. Before the assay, the sample was treated in an ultrasonic bath during 60 s in water with sodium pyrophosphate as dispersing agent, to promote deagglomeration of particles. Results calculated applying Fraunhofer model are shown in Fig. 2.

Fig. 2 shows a wide distribution with a mean value around 9 μm and agglomerates of 30 μm and 100 μm. For this reason, the dispersing agent and the experimental conditions were changed. The sample was mixed with water and a non-ionic surfactant, 0.01% of Tween 80 (Polysorbate 80), as a dispersing agent. In this case, the particle size distribution was calculated using the Mie method. Then, it was treated in an ultrasound bath during 30 s to favor deagglomeration. Particle size distribution calculated by the Mie method can be observed in Fig. 3.

Next experiment, tried to simulate real working conditions in a slurry, microcapsules were dispersed in water and how the particle size distribution changes with time and continuous stirring was evaluated. It is important to notice that stirring takes place during the measurement and for this reason, the sample will disaggregate as time goes by. Three replicates of the same slurry were measured being the time between replicates 30 s. As Fig. 4 shows, the average particle size moved through smaller sizes from 114 μm for the first replicate to 70 μm for the third one. These results demonstrate that aggregates break and the amount of smaller particles increase while bigger ones decrease.

3.1.3. Fourier Transform Infrared spectroscopy (FT-IR)

Fig. 5 shows the analysis by FT-IR spectrum. Peaks from 2954 cm^{-1} to 2850 cm^{-1} correspond to the aliphatic C–H stretching vibration. Vibration at 1728 cm^{-1} is attributed to the carbonyl group of acrylate, while the absorption peak at 1463 cm^{-1} is associated with the C–H bending vibration, and the absorption peak at 1111 cm^{-1} can be assigned to the C–O stretching of the ester group of acrylate.

3.1.4. X-Ray Fluorescence (XRF)

A Micronal® sample was calcined at 500 ºC during 8 h and the composition of the residue was characterized by X-ray fluorescence. Results shown in Table 1 are stated as oxides, and reveal that the major component of this solid is silicon, probably as silicon oxide (93%), and some minor and trace elements as Na_2O, SO_2, and K_2O and CaO.

Silicon may be included in the polymer formulation as SiO_2 as the use of inorganic fillers in polymer formulations is widely described to improve their rigidity; otherwise silicon based compounds like silanes are also added in some polymer formulations, and may lead after a calcining step to SiO_2. With the analytical techniques used it was not possible to identify the silicon compound that origin a SiO_2 residue.

3.1.5. Thermogravimetrical Analysis (TGA)

As observed in the TGA of Micronal® microcapsules depicted in Fig. 6, thermal degradation takes place in two stages. The first one corresponds to the decomposition of the *PCM* paraffin wax between 53 and 202 ºC and the associated loss is 67.17% of the sample. The second mass loss is attributed to the acrylate, and comprises the 23.45% of the Micronal® mass with an onset temperature around 280 ºC. The total loss of ignition at 600 ºC is 90.62% corresponding to the organic components paraffin and acrylate polymer.

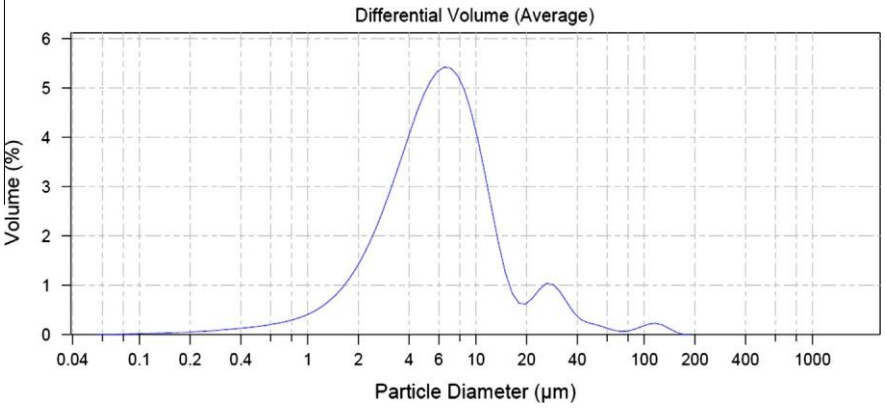

Fig. 2. Particle size distribution of Micronal® DS 5001 calculated using the Fraunhofer model.

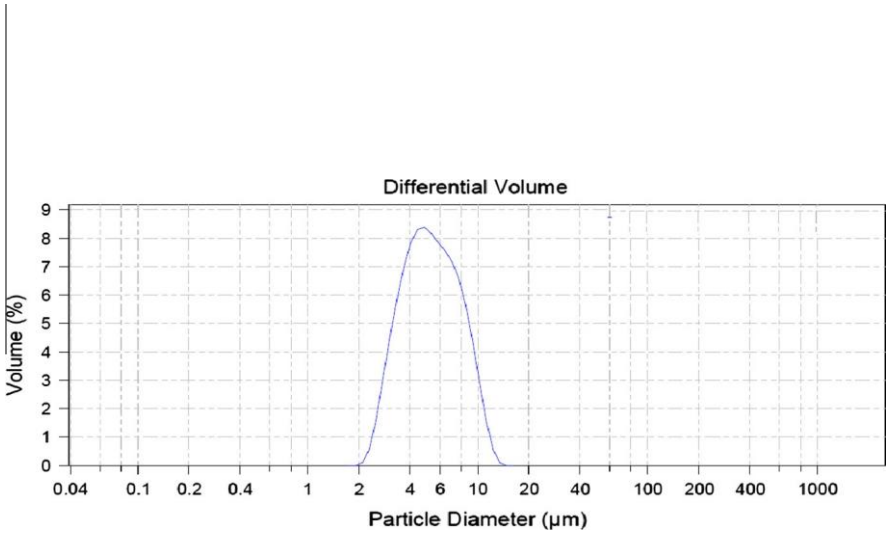

Fig. 3. Particle size distribution of Micronal® DS 5001 using the Mie model.

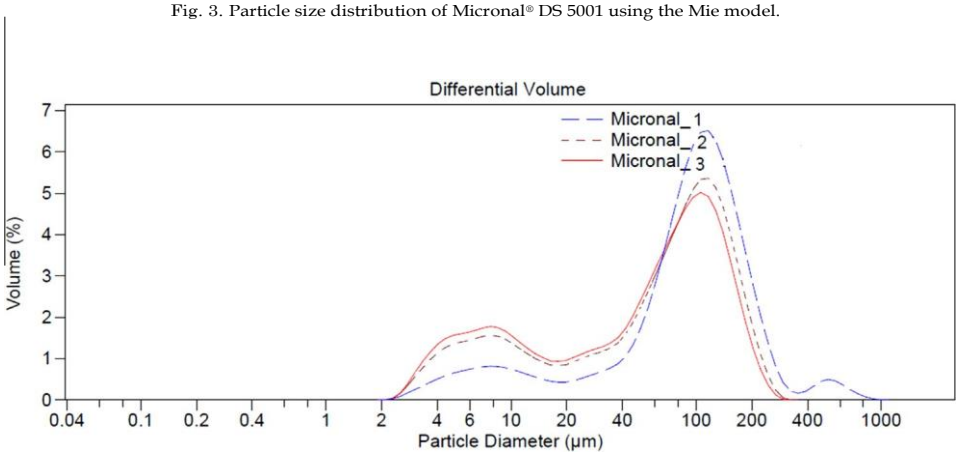

Fig. 4. Comparison of particle size distribution between three replicates with the Mie model.

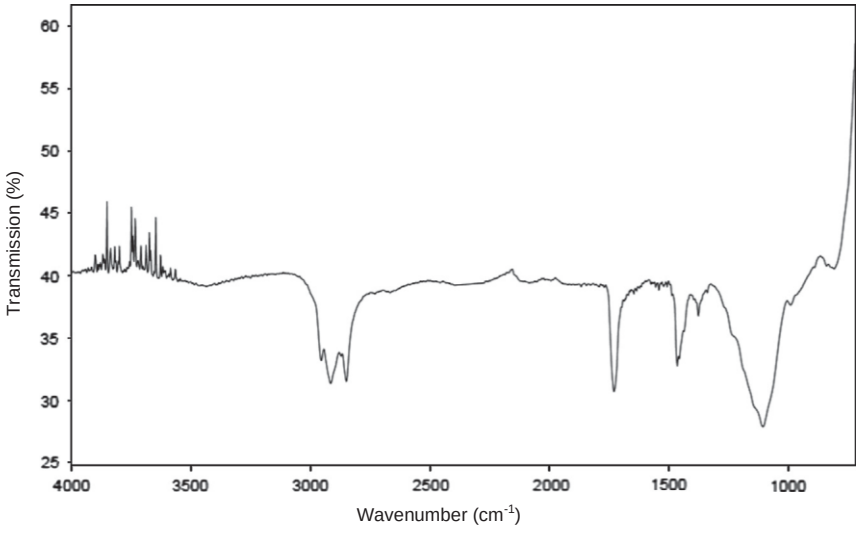

Fig. 5. Fourier transform FT-IR spectra of Micronal® DS 5001.

Table 1
XRF analysis of calcined Micronal® DS 5001, results stated as oxides.

	SiO_2	Na_2O	SO_3	K_2O	MgO	CaO
wt.%	93.0	1.6	0.8	0.3	0.1	0.1

Therefore, the chemical composition of the analyzed Micronal® sample is approximately 67.% paraffin wax PCM, 23% acrylate polymer and 9% of inorganic filler formed mainly by a Si based compound.

3.2. Thermal properties with Differential Scanning Calorimetry (DSC)

Fig. 7a shows the results obtained applying the dynamic method in DSC, where the melting enthalpy is 114.98 kJ/kg, the melting temperature is 27.81 ºC, the solidification enthalpy is 117.85 kJ/kg and the solidification temperature is 26.98 ºC. The results applying the step method are shown in Fig. 7b. The melting enthalpy obtained is 142.55 kJ/kg, the melting temperature is 27.87 ºC, the solidification enthalpy is 137.85 kJ/kg and the solidification temperature is 26.09 ºC.

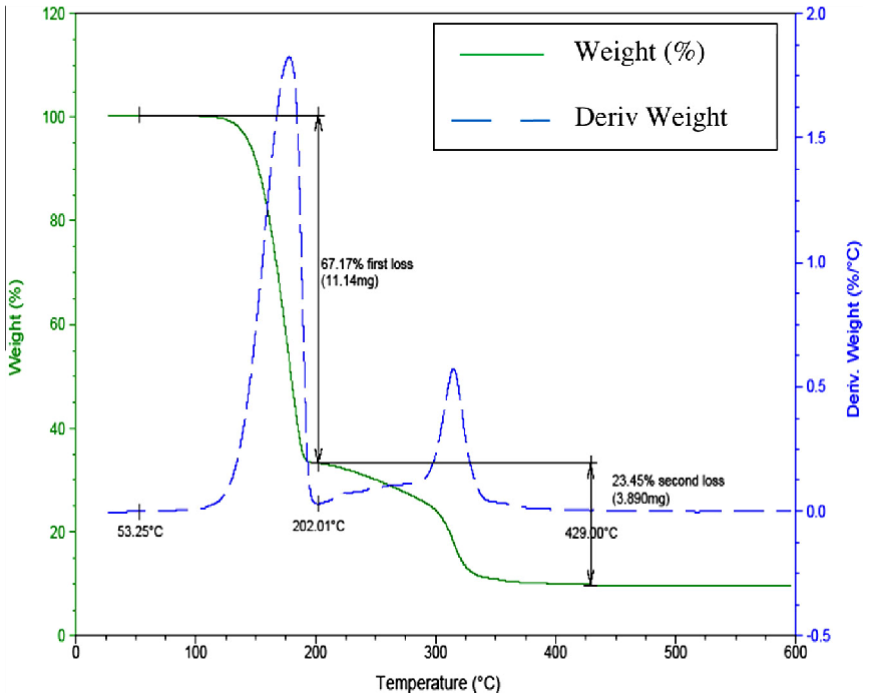

Fig. 6. Thermogravimetrical analysis of Micronal® DS 5001.

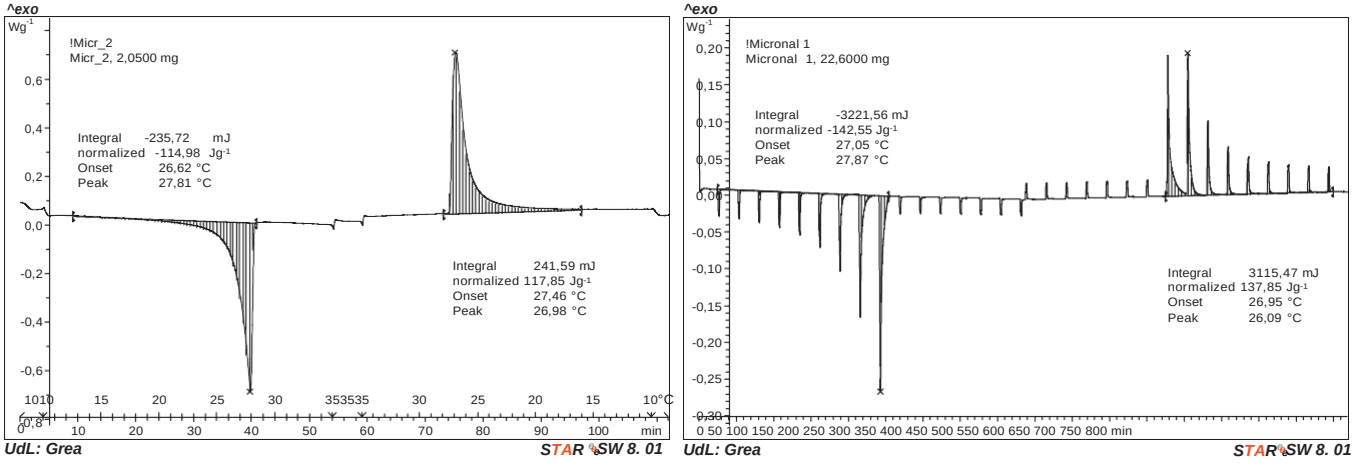

Fig. 7. DSC curves (heat flow vs. time and temperature of the sample) of Micronal® DS 5001 applying, (a) dynamic method (left); and (b) step method (right).

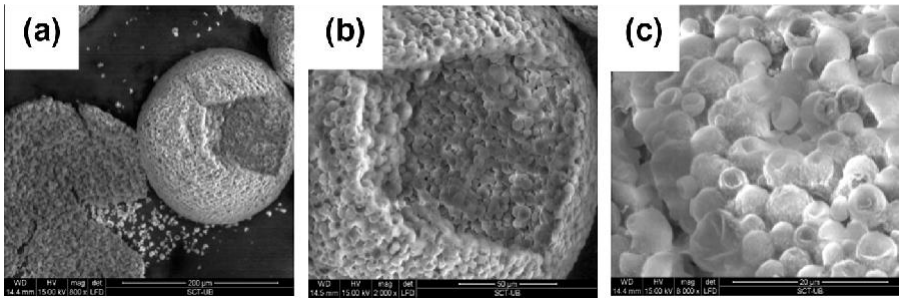

Fig. 8. Micrographies by secondary electron (*SE*) of the sample of Micronal® DS 5001 (a), (b) sample of 150 **1**m and (c) detail of a sphere of 6 **1**m.

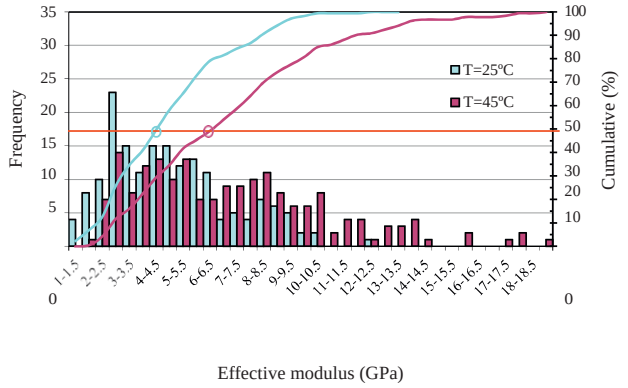

Fig. 9. E_{eff} value of agglomerate particles calculated from AFM nanoindentation experiments at 25 ºC and 45 ºC.

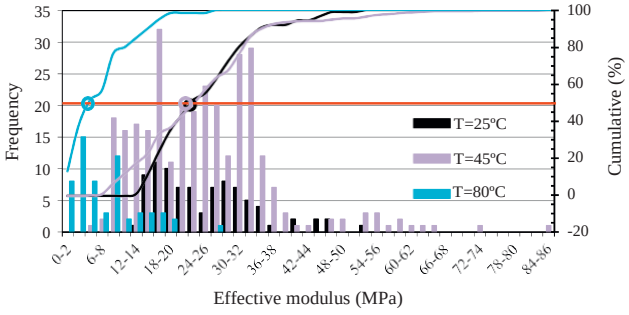

Fig. 10. E_{eff} value of small particles calculated from AFM nanoindentation experiments on Micronal® DS 5001 at 25 ºC, 45 ºC and 80 ºC.

Temperatures of melting and solidification processes are similar comparing the results obtained with both methodologies. Applying both modes, the thermal equilibrium is achieved.

3.3. Scanning Electron Microscopy (SEM)

Fig. 8 shows the morphology and the size of the Micronal® par- ticles. The Micronal® sample consists on microspheres of approximately 150 μm in diameter (Fig. 8a and b), which in turn are made of multiple spheres with diameters approximately 6 μm each (Fig. 8c).

3.4. Stiffness characterization by Atomic Force Microscope (AFM)

Intermittent contact mode topographic images were acquired on the top of the selected particles of 6 μm of Micronal® at 25 ºC, 45 ºC and 80 ºC in order to determine the changes of the sample morphology. It is noticed that particles topography does not change significantly along the phase transition of the core material, indicating that the particles do not break as temperature increases until reaching 45 ºC without any leakage, which would change surface topography.

To determine mechanical properties, 200 nanoindentation experiments were performed by AFM on different spots of the aggregate particles for each tested temperature. It is important to note that every nanoindentation by AFM was performed in a differ- ent spot on the top part of the particle in order to ensure that pre- vious mechanical tests did not change the local mechanical response of the sample. Results are shown in Fig. 9 where the frequency of each result of calculated E_{eff} values is represented.

Results dispersion is due to the extremely local nature of AFM nanoindentation experiments, which are affected by local sample topography, surface defects and tilting and spurious contamination, and this is reflected in elevate standard deviation (s.d.). The E_{eff} mean value at room temperature is 4.9 GPa (s.d. 2.4 GPa) and for the small particles the average value for E_{eff} at 25 ºC was 24.5 MPa, at 45 ºC was 24.9 MPa, and at 80 ºC was 7.4 MPa. In case of small particles, there are no differences in the elastic response at 25 and 45 ºC, but increases significantly at 80 ºC because of this temperature is close to the polymer shell glass transition temperature.

E_{eff} mean value at 45 ºC is 7.2 GPa (s.d. 4.2 GPa). Nevertheless, there is a remarkable increase of E_{eff} at 45 ºC, that is, when the particles core is in liquid phase.

Fig. 10 shows the results obtained on single particles of Micronal® DS 5001. At room temperature the mean value of E_{eff} is 24.5 MPa (s.d. 9.1 MPa) and at 45 ºC, the mean value is 24.9 MPa (s.d. 11.6 MPa). In this case, the results show no significant differences in the elastic response at 25 ºC and 45 ºC. As temperature in creases up to 80 ºC, E_{eff} mean value decreases drastically to 7.4 MPa (s.d. 5.6 MPa). This E_{eff} reduction is attributed to the temperature that is close to the glass transition temperature of acrylate shell (around 100 ºC).

4. Conclusions

Microencapsulated Micronal® DS 5001 consists on paraffinic PCM core and an acrylate outer shell. The solid is made of spherical agglomerates of 150 μm, which are composed of microspheres of 6 μm in size (small particles). The chemical composition of the sample is approximately 67% paraffin wax PCM, 23.5% acrylate polymer, and 9% of a Si based compound. The material shows a phase change temperature range between 26.09 ºC and 27.81 ºC. The latent heat shows a melting enthalpy between 114.98 kJ/kg and 142.55 kJ/kg and a solidification enthalpy between 117.85 and 137.85 kJ/kg.

Different values were obtained for E_{eff} depending on the size of the particle and the temperature. For agglomerates the average value for E_{eff} at 25 ºC was 4.9 GPa, and at 45 ºC was 7.2 GPa. Besides,

Acknowledgements

The work is partially funded by the Spanish government (ENE2011-28269-C03-02 and ENE2011-22722) and the European Union (COST Action TU0802). The authors would like to thank the Catalan Government for the quality accreditation given to their research group GREA (2009 SGR 534) and research group DIOPMA (2009 SGR 645).

References

[1] Joulin A, Younsi Z, Zalewski L, Lassue Z, Rousse DR, Cavrot JP. Experimental and numerical investigation of a phase change material: thermal-energy storage and release. Appl Energy 2011;88(7):2454–62.
[2] Castellón C, Martorell I, Cabeza LF, Fernández AI, Manich AM. Compatibility of plastic with phase change materials (PCM). Int J Energy Res 2010;35:765–71.
[3] Bayés-García L, Ventolà L, Cordobilla R. Phase change materials (PCM) microcapsules with different shell compositions: preparation, characterization and thermal stability. Sol Energy Mater Sol Cells 2010;94:12535–40.
[4] Zhou D, Zhao CY, Tian Y. Review on thermal energy storage with phase change materials (PCMs) in building applications. Appl Energy 2012;92:593–605.
[5] Zhou G, Yang Y, Xu H. Performance of shape-stabilized phase change material wallboard with periodical outside heat flux waves. Appl Energy 2011;88(6):2113–21.
[6] Oró E, de Gracia A, Castell A, Farid MM, Cabeza LF. Review on phase change materials (PCMs) for cold thermal energy storage applications. Appl Energy 2012;99:513–33.
[7] Cai Y, Wei Q, Huang F, Gao W. Preparation and properties studies of halogen-free flame retardant form-stable phase change materials based on paraffin/high density polyethylene composites. Appl Energy 2008;85(8):765–75.
[8] Kravvaritis ED, Antonopoulos KA, Tzivanidis C. Experimental determination of

the effective thermal capacity function and other thermal properties for various phase change materials using the thermal delay method. Appl Energy 2011;88(12):4459–69.
[9] Rao Z, Wang S, Peng F. Self diffusion of the nano-encapsulated phase change materials: a molecular dynamics study. Appl Energy 2012.
[10] Li M, Wu Z, Kao H. Study on preparation, structure and thermal energy storage property of capric-palmitic acid/attapulgite composite phase change materials. Appl Energy 2011;88(9):3125–32.
[11] Wang L, Meng D. Fatty acid eutectic/polymethyl methacrylate composite as form-stable phase change material for thermal energy storage. Appl Energy 2010;87(8):2660–5.
[12] Li M, Kao H, Wu Z, Tan J. Study on preparation and thermal property of binary fatty acid and the binary fatty acids/diatomite composite phase change materials. Appl Energy 2011;88(5):1606–12.
[13] Cai Y, Ke H, Dong J, Wei Q, Lin J, Zhao Y, et al. Effects of nano-SiO2 on morphology, thermal energy storage, thermal stability, and combus- tion properties of electrospun lauric acid/PET ultrafine composite fibers as form-stable phase change materials. Appl Energy 2011;88(6): 2106–12.
[14] Chen ZH, Yu F, Zeng XR, Zhang ZG. Preparation, characterization and thermal properties of nanocapsules containing phase change material n-dodecanol by miniemulsion polymerization with polymerizable emulsifier. Appl Energy 2012;91(1):7–12.
[15] Tyagi VV, Kaushik SC, Tyagi SK, Akiyama T. Development of phase change materials based microencapsulated technology for buildings: a review. Renew Sust Energy Rev 2011;15:1373–91.
[16] Farid MM, Khudhair AM, Razack SAK, Al-Hallaj S. A review on phase change energy storage: materials and applications. Energy Convers Manage 2004;45:1597–615.
[17] Chen B, Wang X, Zeng R, Zhang Y, Wang X, Niu J, et al. An experimental study of convective heat transfer with microencapsulated phase change material suspension: laminar flow in a circular tube under constant heat flux. Exp Therm Fluid Sci 2008;32:1638–46.
[18] Sari A, Alkan C, Karaipekli A, Uzun O. Microencapsulated n-octacosane as a phase change material for thermal energy storage. Sol Energy 2009;83:1757–63.
[19] Khudhair AM, Farid MM. A review on energy conservation in building applications thermal storage by latent heat using phase change materials. Energy Convers Manage 2004;45:263–75.
[20] Cabeza LF, Castel A, Barreneche C, de Gracia A, Fernández AI. Materials used as PCM in thermal energy storage in buildings: a review. Renew Sust Energy Rev 2011;15:1675–95.
[21] Su JF, Wang LX, Ren Li. Preparation and characterization of double-MF shell microPCMs used in building materials. J Appl Polym Sci 2005;97(5): 1755–62.
[22] Heinz A, Streicher W. Application of phase change materials and PCM-slurries for thermal energy storage. In: 10th International conference on thermal energy storage, Stockton; 2006.
[23] Zhang GH, Zhao CY. Thermal and rheological properties of microencapsulated phase change materials. Renew Energy 2011;36:2959–66.
[24] Yang R, Xu H, Zhang Y. Preparation, physical property and thermal physical property of phase change microcapsule slurry and phase change emulsion. Sol Energy Mater Sol Cells 2003;80:405–16.
[25] Hu X, Zhang Y. Novel insight and numerical analysis of convective heat transfer enhacement with microencapsulated phase change material slurries: laminar flow in a circular tube with constant heat flux. Int J Heat Mass Trans 2002;45:3163–72.
[26] Delgado M, Lázaro A, Mazo J, Marín JM, Zalba B. Experimental analysis of a microencapsulated PCM slurry as thermal system and as heat transfer fluid in laminar flow. Appl Therm Eng 2012;36(1):370–7.
[27] Lu W, Tassou SA. Experimental study of the thermal characteristics of phase change slurries for active cooling. Appl Energy 2012;91(1):366–74.
[28] Delgado M, Lázaro A, Mazo J, Zalba B. Review on phase change material emulsions and microencapsulated phase change material slurries: materials heat transfer studies and applications. Renew Sust Energy Rev 2012;16(1):253–73.
[29] Zhang Y, Wang S, Rao Z, Xie J. Experiment on storage characteristic of microencapsulated phase change material slurry. Sol Energy Mater Sol C2011;95(10):2726–33.
[30] Diaconu BM, Varga S, Oliveira AC. Experimental assessment of heat storage properties and heat transfer characteristics of a phase change material slurry for air conditioning applications. Appl Energy 2010;87(2):620–8.
[31] de Boer GBJ, de Weerd C, Thoenes D, Goossens HWJ. Laser diffraction spectrometry: Fraunhofer diffraction versus Mie scattering. Part Syst Charact 1987;4:14–9. http://dx.doi.org/10.1002/ppsc.19870040104.
[32] Marin JM, Zalba B, Cabeza LF, Mehling H. Determination of enthalpy- temperature curves of PCM with the *t*-history method – improvement to temperature dependent properties. Meas Sci Technol 2003;14:184–9.
[33] Mehling H, Cabeza LF. Heat and cold storage with PCM. Springer-Verlag; 2008. ISBN-13: 9783540685562.
[34] Florin EL, Rief M, Lehmann H, Ludwig M, Dornmair C, Moy VT, et al. Sensing specific molecular-interactions with the atomic-force microscope. Biosens Bioelectron 1995;10:895–901.
[35] Namazu T, Isono Y. Quasi-satic bending test of nano-scale SiO_2 wire at intermediate temperatures using AFM-based technique. Sensor Actuator A 2003;194:78–85.
[36] Oliver WC, Pharr GM. An improved technique for determining hardness and elastic modulus using load and displacement sensing indentation experiments. J Mater Res 1992;7(6):1564–83.
[37] Rothon RN. Mineral fillers in thermoplastics: filler manufacture and characterisation. Adv Polym Sci 1999;139:67–107.